

Exploring the Chemistry of Low-Temperature Ignition by Pressure-Accelerated Dynamics

Lukas Krep,^[a] Wassja Alexander Kopp,^[a] Leif Christian Kröger,^[a] Malte Döntgen,^[a, b] and Kai Leonhard*^[a]

Reaction models that accurately describe the complex reaction processes of ignition are key for the development of novel engine- and fuel concepts. Since reactive molecular dynamics can be used to discover reaction networks in a largely automated fashion, this method has the potential to drastically reduce the real time effort necessary for the development of reaction models. With standard reactive molecular dynamics, the simulation of low-temperature reaction processes is hindered by the small accessible time scales of only a few

nanoseconds. In this work, we propose the pressure-accelerated dynamics method to overcome the time scales obstacle through exploitation of Le Chatelier's principle. For the example of pentane low-temperature ignition, we show that with pressure-accelerated dynamics, the ReaxFF reactive force field, and the ChemTraYzer not only the known key low-temperature ignition pathways can be found, but also reactions that are not yet included in reaction models.

1. Introduction

For the design of spark-ignition (SI) and compression-ignition (CI) engines as well as for the development of novel engine concepts, detailed knowledge about the ignition process is required.^[1,2] However, ignition processes, like many other chemical processes, such as catalyzed saccharides conversion,^[3] or polymerization,^[4] are complex phenomena with a variety of species and reactions to be modeled, cf. e.g. the reaction models by Bugler et al.,^[5–7] or Ranzi et al..^[8]


As the automatization of the time-consuming task to develop reaction models is highly desirable, a number of automated approaches have been proposed, such as Reaction Mechanism Generator,^[9] AutoTST,^[10] EXGAS,^[11] Rule Input Network Generator,^[12] KinBot,^[13] the Heuristics-Guided Exploration of Reaction Mechanisms by Bergeler et al.,^[14] or molecular graph methods.^[15–20] A discussion of recent advances in reaction network exploration methods is given by Dewyer et al..^[21] For many fuels, these methods are already able to estimate kinetic and thermodynamic models. Clearly, only reactions included in the applied heuristics, e.g. reaction classes,^[9] chemical descriptors,^[14] can be expected to be found.^[22] Other approaches, such as ADDF,^[23,24] or GRRM,^[25] do not simplify


chemical space using heuristics but are limited in applicability to smaller systems due to their high computational cost.^[21] Reactive molecular dynamics (rMD) is an alternative approach to determine reaction networks that does not rely on predefined classes and heuristics, but is able to handle large complex systems. The ability to predict reaction networks, kinetics, and thermochemistry makes rMD methods interesting for the generation of reaction mechanisms, as they need less or ideally even no *a-priori* knowledge.

As feasible timescales of rMD simulations are limited to a few nanoseconds, some reaction processes, such as low-temperature ignition (600–900 K), are too slow by several orders of magnitude to be fully uncovered by standard rMD at engine-relevant conditions. In the last two decades, a number of acceleration methods have been developed in order to extend feasible timescales. One group of methods includes the hyperdynamics,^[26] metadynamics,^[27] bond-boost,^[28] or the Collective Variable-Driven Hyperdynamics (CVHD)^[29] methods. These methods apply bias potentials to reduce potential energy barriers. Another group includes the Temperature-Accelerated Dynamics (TAD) method,^[30] which adds kinetic energy distributed randomly over all configurations by an increase of temperature, or the Forward Flux Sampling (FFS) method^[31–34] that adds kinetic energy only to configurations specified by an order parameter. Another possibility to increase the observation probability of infrequent events, such as reaction events, is the exploitation of parallelization as in the parallel replica method.^[35,36] With the existing methods, it is possible to extend feasible timescales by multiple orders of magnitude.^[29] They have been shown to be applicable to a great variety of problems.^[37–45] Still, there are limitations to these methods. It has been found, for example, that the construction of bias potentials is not trivial.^[46] For each system of interest the metadynamics user is confronted with the task of choosing a collective variable that delivers the necessary acceleration for the desired transitions and at the same time does not block

[a] L. Krep, Dr. W. A. Kopp, L. C. Kröger, Dr. M. Döntgen, Prof. Dr. K. Leonhard
Institute of Technical Thermodynamics, RWTH Aachen University, Aachen
52062, Germany
E-mail: kai.leonhard@ltt.rwth-aachen.de

[b] Dr. M. Döntgen
School of Engineering, Brown University, Providence, RI 02912, USA

 An invited contribution to a Special Collection on the Computational Chemistry of Complex Systems

 ©2019 The Authors. Published by Wiley-VCH Verlag GmbH & Co. KGaA.
This is an open access article under the terms of the Creative Commons Attribution License, which permits use, distribution and reproduction in any medium, provided the original work is properly cited.

relevant but often *a-priori* unknown parts of chemical space. It has been shown that the effort to find an appropriate collective variable can be alleviated but not fully overcome using deep learning methods as the employed method requires training for each application.^[47] Originally, the bond-boost method was designed to accelerate bond breaking,^[28] but the method has been extended to accelerate both bond breaking and forming of pre-defined atoms.^[45] In processes, such as low-temperature ignition, in which the reactivity is determined by meta-stable reaction equilibria (O_2 -addition), and slow subsequent reactions (internal H-atom abstraction, cf. Figure 1), acceleration methods should push the reaction equilibrium to the product side to increase the probability of observing subsequent reactions, which the bond-boost method does not achieve. For a similar reason, the use of TAD is not advisable for the rMD simulation

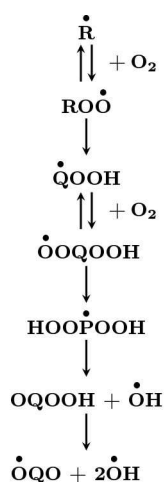


Figure 1. The key low-temperature chain branching path starting from the alkyl radical $\dot{\text{R}}$. A detailed review on low-temperature ignition chemical processes can be found in Zador et al.^[2]

of low-temperature ignition processes. The use of high temperatures pushes the meta-stable O_2 -addition reaction equilibrium to the reactant side. The shift of the O_2 -addition reaction equilibrium to the reactant side diminishes the number of peroxy-radicals that can undergo further low-temperature reactions (e.g. internal H-atom abstractions, cf. Figure 1 for a skeletal mechanism). The decreasing number of peroxy-species counteracts the accelerating effect of increasing temperature on subsequent reactions and leads to an increase in ignition delay at certain temperatures (cf. Figure 2). A further increase of temperature eventually paves the way for pyrolysis and other reactions with high-energy reaction barriers. That means, at sufficiently high temperatures, the ignition delay decreases again. This complicated interplay of shifts in O_2 -addition reaction equilibria and acceleration of high-barrier reactions leads to s-shaped ignition delay time graphs (cf. Figure 2) for many hydrocarbons. A pronounced increase of ignition delay is called “Negative-Temperature Coefficient” (NTC) behavior. Figure 2 shows ignition delay times for different initial temperatures and pressures for lean pentane-oxygen mixtures with an equivalence ratio of $\phi = 0.09$. At the lowest temperatures, e.g. below 800 K at 10 atm, ignition is dominated by O_2 -additions and internal H-atom abstractions.^[2] At the lowest pressures this mixture shows NTC behavior. From the pronounced NTC behavior, two more regimes besides the low-temperature regime can be identified that come along with the described changes in O_2 -addition reaction equilibria and a change in predominant reactions from low-temperature reactions to high-temperature reactions (e.g. pyrolysis) – the intermediate and the high-temperature regime. According to mechanistic simulations the NTC behavior becomes less pronounced with increasing pressure, until it eventually vanishes at pressures between 250 atm and 1250 atm (cf. Figure 2). At the highest pressures after the NTC behavior has vanished, both low-temperature and high-temperature reactions remain present.

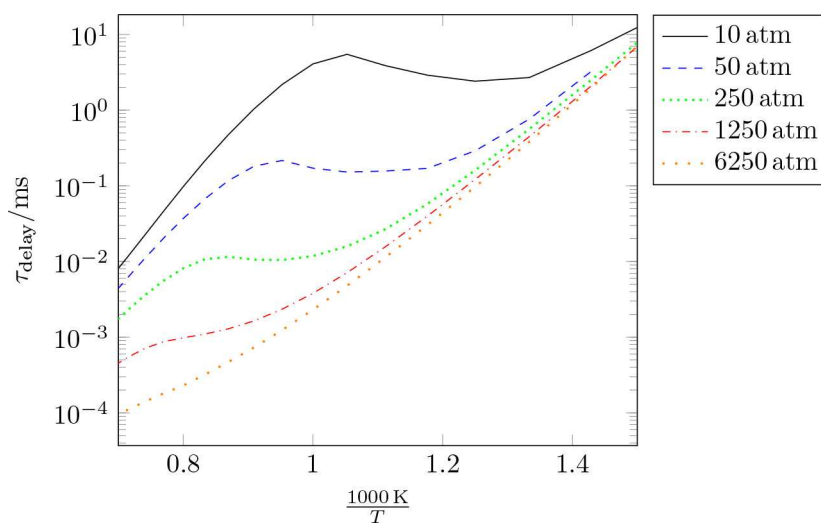


Figure 2. Ignition delay time of *n*-pentane for different initial pressures modeled with the reaction mechanism from Bugler et al.^[7,6,5] in adiabatic isochoric simulations. The simulations were conducted with Cantera.^[50] Ignition delay times of lean *n*-pentane-oxygen mixtures with an equivalence ratio of $\phi = 0.09$ as in our rMD simulations are shown.

These findings are qualitatively validated by high-pressure experiments up to 530 atm.^[48] An overview of important reactions in all three regimes can be found in Curran et al.^[49]

Besides a vanishing NTC behavior, we observe that the low-temperature regime extends to higher temperatures and shorter ignition delay times with increasing pressure. The observation that with pressure the low-temperature ignition is accelerated and the low-temperature regime extends to higher temperatures is important as it leads to the idea to use elevated pressures to accelerate rMD simulations of low-temperature ignition. In other words, we propose to modify the standard MD approach from searching for the phenomena that are present at specific conditions to finding conditions that allow for the observation of such phenomena. Certainly, this requires more *a-priori* knowledge than the set-up of a standard MD simulation but compared to the aforementioned bias-potential acceleration methods no detailed knowledge of the underlying processes on the atomic scale is required. In case of ignition, which is presented in this work, the observation that the ignition process is generally accelerated with increasing pressure (cf. Figure 2) is a sufficient motivation to run rMD simulations at elevated pressure. Still, knowledge of the most important reactions is helpful to find a set-up, which increases the probability to observe the expected reactions. The key idea of the method presented in this work is to increase the partial pressures of the reactants. That way, the reaction equilibria of the O₂-addition reactions, which are key reactions in the low-temperature ignition process, are pushed to the product side. Hence, the product, the peroxy radical, is available for a larger part of the simulation and thus the probability to observe subsequent reactions, such as the internal H-atom abstraction, is increased. The extension to higher temperatures is another important ingredient of the “pressure-accelerated dynamics” (pAD) method as it allows to accelerate reactions subsequent to the O₂-addition not only by the increase of reactant concentration, but also by temperature. A similar approach has already been employed in the nanoreactor.^[51] They use a virtual piston to increase the pressure periodically.^[51] As the authors note, their goal is to find reactions that are generally possible on the given potential energy surface instead of generating kinetic models that are consistent with any given temperature and density directly. Meaningful kinetics have to be generated through reoptimization of barrier heights and thermochemistry using DFT or higher-level methods and subsequent reaction model building. Only then, the kinetics are extrapolatable to other temperatures. With pAD, consistent high-pressure limit kinetics are directly generated for the simulated conditions. With a second set of pAD simulations at different temperatures, extrapolation of the kinetics is possible without the need of reoptimizations. Apart from the periodically high concentrations in the nanoreactor, equilibrium simulations with high concentrations have already been successfully used to accelerate high-temperature oxidation and pyrolysis in ReaxFF studies,^[52] the oxidation of cyclohexane and other systems using metadynamics and the GFN2-xtb hamiltonian.^[53] Bal and Neyts^[54] use the CVHD acceleration method and ReaxFF to investigate the oxidation processes of *n*-dodecane. From their simulations, they

note that the average reaction time decreases with pressure. In our work, we exploit this observation for acceleration purposes and show that an increase in pressure is already sufficient to observe low-temperature ignition reaction pathways. We present pAD as a method predestined to investigate low-temperature ignition processes. Nevertheless, the applicability of pAD is not limited to low-temperature ignition processes but can more generally be used for systems in which association reactions in the gas phase are expected to play a key role. As pAD does not require any code implementation or construction of a bias potential, it is not only very convenient to use but can also easily be combined with other acceleration methods, e.g. metadynamics.^[53] As an example, we present the low-temperature reaction pathways observed during pAD simulations of pentane low-temperature ignition processes using the ReaxFF reactive force field.^[55] It will be shown that inaccuracies of the ReaxFF force field can have a considerable impact on the branching ratios. Still, with ReaxFF, we are able to find the expected, important low-temperature reactions, and other side reactions, whose importance for reaction models might have been overlooked so far.

Computational Methods

The alkyl radical and especially the oxygen concentration c_{O_2} are the key parameters here. A higher concentration of these two species pushes the reaction equilibrium of the O₂-addition to the product side, i.e. the peroxy radical. As the peroxy concentration is thereby increased, the subsequent reactions, most notably the internal H-atom abstraction (cf. Figure 1), are accelerated. For the optimal choice of the simulation box composition and the simulation temperature in NVT simulations, the existence of reactions parallel to the reactions we intend to observe, especially the O₂-addition and the internal H-atom abstraction, must be taken into account. The β -scission is the most important parallel reaction that becomes competing with the O₂-addition. That means, the β -scission reaction rate constant $k_{\beta\text{-scis}}$ is of the same order of magnitude as the pseudo-first-order reaction rate constant $k_{O_2\text{-add}} \cdot c_{O_2}$. Figure 3 illustrates that an increase of c_{O_2} by two orders of magnitude ($0.0001 \text{ mol cm}^{-3}$ – 0.01 mol cm^{-3}) shifts the temperatures at which the β -scission and the O₂-addition are competing from less than 1200 K to more than 1800 K (cf. the areas left of the vertical lines in Figure 3). A c_{O_2} of $0.0001 \text{ mol cm}^{-3}$ corresponds to the oxygen concentration of a stoichiometric ideal pentane-oxygen mixture at approx. 10 atm.

To increase the reaction rate of the O₂-addition, we could also increase the alkyl radical concentration. An increase of the alkyl radical concentration would also increase the reaction rate of the β -scission, though. Therefore, we decided to choose a highly diluted system. In order to focus on the key low-temperature reactions, we decided to put only one fuel radical into the simulation box. A side effect of the high dilution is that self-interactions, which might appear in small boxes with periodic boundary conditions, are shielded by the large number of O₂ molecules. The box size was adjusted to fit the respective c_{O_2} . The appropriate order of magnitude of O₂ concentration depends on the simulation temperature. For the choice of temperature, we take the most important parallel ROO reactions in the low-temperature chain-branching process (cf. Figure 1) into account (cf. Figure 4). In the high-pressure limit, the reaction rate constants of the internal H-atom abstraction $k_{\text{int H-atom abstr}}$ and the reverse reaction of the O₂-addition, the R–O₂

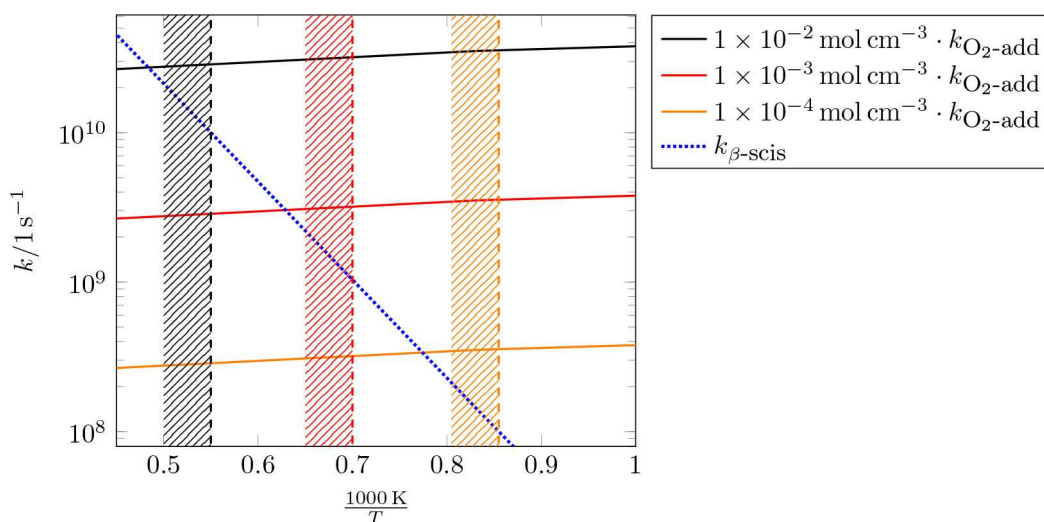


Figure 3. The gap between the high-pressure limit pseudo-first-order reaction rate constants of the O_2 -addition reaction $k_{O_2-add} \cdot c_{O_2}$ and the reaction rate constant of the β -scission $k_{\beta-scis}$ of the 2-pentyl radical is shown for different oxygen concentrations c_{O_2} . O_2 -addition rate constants are taken from Asatryan and Bozzelli,^[56] the β -scission rate constants from Comandini et al..^[57] At temperatures left of the vertical lines β -scissions are competing to the pseudo-first-order reaction rate constants with a c_{O_2} of the same color or even become dominating.

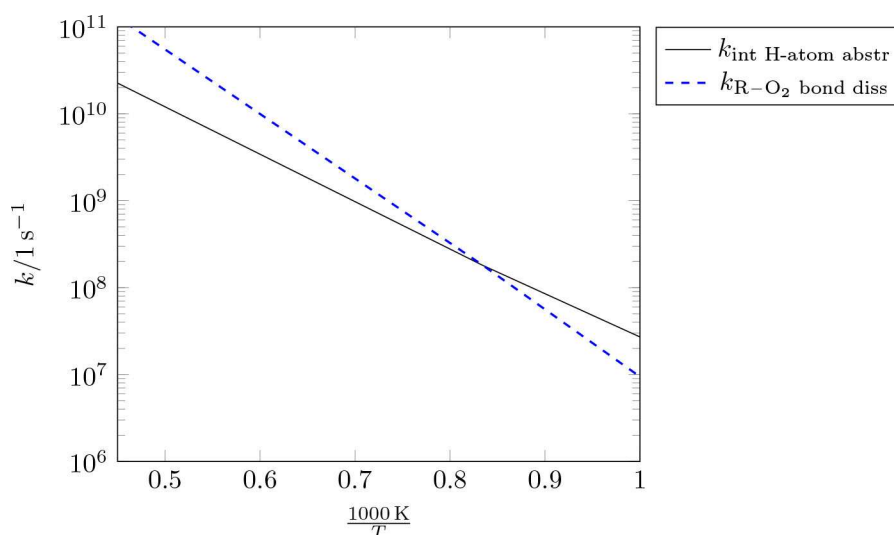


Figure 4. The reaction rate constants of the first internal H-atom abstraction and the reaction rate constant of the R- O_2 bond dissociation reaction of the 2-peroxide-pentane, obtained from Asatryan and Bozzelli,^[56] intersect at approx. 1200 K.

bond dissociation, $k_{R-O_2 \text{ bond diss}}$ only depend on the temperature. $k_{\text{int H-atom abstr}}$ and $k_{R-O_2 \text{ bond diss}}$ intersect at approx. 1200 K. Below, $k_{\text{int H-atom abstr}}$ is higher than $k_{R-O_2 \text{ bond diss}}$. In this regard, temperatures lower than 1200 K are preferable for the simulation of low-temperature ignition processes. On the other hand, for the chosen box composition with one fuel radical, which means, there will also be only one C5 peroxy radical in the box, we have to simulate at higher temperatures than 1200 K to achieve expected waiting times of less than 10 ns for the internal H-atom abstraction to occur at least once with a 90% observation probability. A derivation for the expected waiting time can be found in Kröger et al..^[58] Our considerations show that for the choice of temperature a trade-off between a low reactivity of reactions subsequent to O_2 -additions at low temperatures and increasing importance of R- O_2 bond dissociations, and β -scissions at high temperatures is necessary.

With a c_{O_2} of 0.01 mol cm^{-3} , $k_{O_2-add} \cdot c_{O_2}$ is more than two orders-of-magnitude larger than $k_{\beta-scis}$ at 1200 K, which gives us a safety margin in case the β -scission is faster and the O_2 -addition is slower than expected in our simulations. Also, at 1200 K R- O_2 bond dissociations are at least not faster than the internal H-atom abstraction, making 1200 K a possible trade-off. Choosing pentane ignition as case study allowed us to determine favorable NVT simulation conditions from literature reaction rate constants.^[56,57] The chosen simulation conditions should be transferable to other fuels, as the change in regimes in the ignition delay time often appears at similar temperatures (cf., [59–61] a comparative plot is given in the Supporting Information).

We have conducted 200 simulations with 90 oxygen molecules and one pentane molecule ($\phi = 0.09$) in the simulation box at 1200 K. The simulation boxes were created with packmol.^[62] After a

minimization and a thermalization of 500 ps, we removed an H-atom from the pentane molecule and from the system. That means, the analyzed part of the trajectory with a length of approx. 2 in total starts with a 2-pentyl radical. Simulations were run using the USER-REAXC package and fix qeq/reax^[63] implemented in LAMMPS version 17Nov16^[64] and were analyzed with the ChemTraYzer.^[65] The simulations were thermostated with the Nose-Hoover thermostat implemented in LAMMPS with a damping constant of 10 fs. A timestep of 0.1 fs was used. Back and forth reactions occurring within 1 ps were considered to be recrossing events and were therefore not counted.

We chose the well-established CHO-2008 parametrization by Chenoweth et al.,^[55] which has been designed to study combustion processes. The CHO-2008 parametrization has been applied to various systems.^[66–74] For all these cases, “generally a good agreement with experimental results in terms of the initiation mechanism and barriers were observed”.^[52] Comparison of the bond dissociation energies of the species used in the training data (ReaxFF bond dissociation energies vs. B3LYP bond dissociation energies, cf. Chenoweth et al.^[55]) shows that we have to expect average errors of more than 10 kcal mol^{−1} in bond dissociation energies. We use the bond dissociation energy error as an estimate for the reaction barrier error of the force field. For the GMTKN55 database an error of 3.2 kcal mol^{−1} was reported for barrier heights for B3LYP.^[75]

In order to verify observed reaction paths, transition state theory (TST) reaction rate constants were calculated using the RRHO model implemented in tamkin.^[76] Transition states were optimized with the Berny algorithm^[77] implemented in Gaussian09 at the CBS-QB3^[78,79] level of theory. The CBS-QB3 model chemistry has been evaluated on test sets, e.g. in the DBH24/08 database of barrier heights. Therein, Zheng et al.^[80] report an error of 1.62 kcal mol^{−1} in CBS-QB3 barrier heights. Additional uncertainty arises from the other RRHO ingredients of the TST rate constant formulation. Kopp et al.^[81] evaluated these uncertainties for B3LYP geometries and frequencies, which are also used in CBS-QB3. Combining these uncertainties with the uncertainty in barrier height leads to an uncertainty in the rate constants of a factor of 10 at 1000 K. By rotating C–C and C–O single bonds, conformers were searched on the B3LYP/CBSB7 level of theory, which is also used for geometry optimizations and frequency calculations in the CBS-QB3 compound method.^[78] Transition states on ReaxFF level were optimized with an in-house python implementation of the Berny algorithm.^[77] Additionally, we conducted rMD simulations in a temperature range from 1200 K up to 1450 K in steps of 50 K (10 simulations per temperature) for comparison of reaction rate constants.

All simulations with the model by Bugler et al.^[5–7] (cf. Figures 2, 5) were conducted with Cantera^[50] and the IdealGasReactor model. Simulation conditions are given in the Figure captions.

2. Results and Discussion

Figure 5 shows the lumped reaction scheme of the low-temperature chain branching mechanism with branching ratios of C5 species from our simulations and from the reaction model by Bugler et al.^[5–7] applied at 1300 atm. A detailed list of observed reactions is provided in the Supporting Information. In order to obtain the depicted branching ratios in Figure 5, isomers were first lumped into species classes. As the internal H-atom abstraction is an important reaction in the low-temperature ignition process, the peroxy radicals and the hydroperoxy radicals were lumped into two different species classes. Unlike

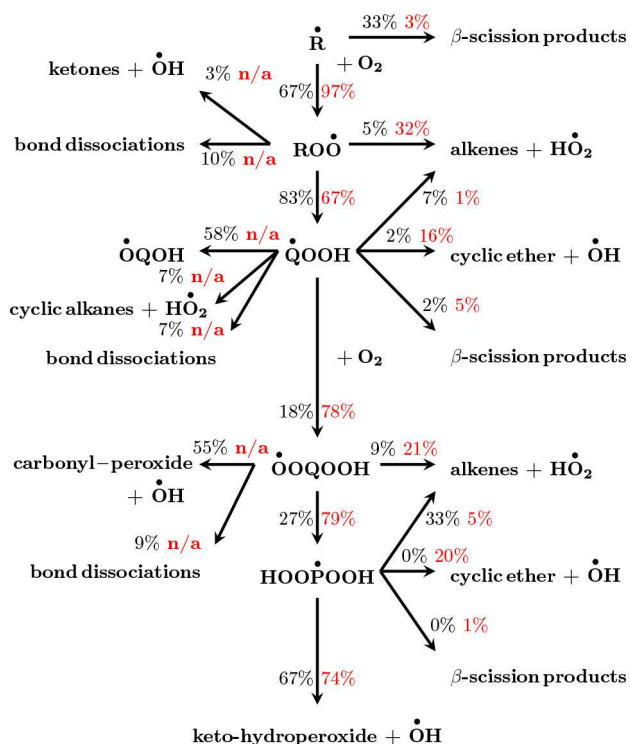


Figure 5. Lumped C5 reaction scheme with branching ratios from our simulations (black) and from the model by Bugler et al.^[5–7] (red) at 1200 K, 1300 atm and up to 1% fuel consumption. Fluxes are derived from lumping all isomers to classes of species. Thus, isomerizations, except internal H-atom abstractions and the OH-migration ($ROO^\bullet \rightarrow QOOH$, $QOOH \rightarrow QOQOH$, $QOQOOH \rightarrow HOOPOOH$), are not taken into account. Fluxes obtained from simulations with the reference model are time-averages over the simulation time up to 1% fuel consumption.

$QOOH$, $QOQOH$ species do not follow the key reaction path anymore. Therefore, also $QOOH$ and $QOQOH$ are separate species classes. Branching ratios were then obtained by dividing the net number of escaping reaction events from one species class into another $N_{\text{forward}} - N_{\text{backward}}$ by the sum of all net number of reaction events that escape from one species class. For consistency, the fluxes generated with the reference model, from which the reference branching ratios have been obtained are averaged over the simulation time up to 1% fuel consumption. 1% fuel consumption is a trade-off between 20% fuel consumption, which usually serves as the reference time for the rate-of-progress analysis (cf. [6,82]) and the initial, pre-ignition reactor composition, which is represented by our MD set-up (low fuel radical concentration). Assuming only the uncertainty of the dissociation energies of 10 kcal mol^{−1} to be present in barrier heights, we already obtain substantial uncertainties in the branching ratios. Hence, the branching ratios shown here can only serve as an orientation, whether the simulations produced mostly reasonable results, i.e. the majority of observed reactions are members of well-known reaction classes. The error propagation scheme is given in the Supporting Information. It should be mentioned that also the reference branching ratios must be expected to have uncertainties given the high pressure. Rigorously, real-gas effects would

have to be considered. Here, we neglect them for two reasons. First, Zhukov^[48] showed for the *n*-heptane model by Curran et al.^[49] that only marginal reoptimizations of reaction rate constants are required to adjust the reaction model to high pressures. Second, as already argued, the branching ratios are only for qualitative comparison considering the large uncertainties in the MD branching ratios. To resolve the largest deviations between reaction pathways from our simulations and from the model by Bugler et al.^[5–7] we recalculated the 2-pentyl radical → 2-methyl-but-1-yl radical isomerization and the OH-migration of the 2-hydroperoxide-pent-4-yl radical with quantum mechanical methods as described above (cf. Figures 6, 7). For the identification of reactions that require further attention, the magnitude of the uncertainty in the free-energy reaction barrier can be used as an alternative.^[83] The approach

by Proppe et al.^[83] can be used for a system-specific reparametrization of the force field.^[83]

As expected, a majority of the initial pentyl radicals proceeds through the first O₂-addition in our simulations (67 %), while the rest proceeds through β -scissions. Before proceeding through these reaction channels, in many simulations the 2-pentyl radical isomerizes first, mainly to the 2-methyl-but-1-yl radical. Intuitively, the branching ratio of the isomerization to the 2-methyl-but-1-yl radical of 41 % seems to be very high compared to O₂-additions and β -scissions. Comparison of reaction rate constants derived from MD trajectories and CBS-QB3 TST reaction rate constants in Figure 6 shows that the MD reaction rate constants of the isomerization $k_{\text{Iso,ReaxFF}}$ are approximately seven orders-of-magnitude higher than the TST reaction rate constants $k_{\text{Iso,TST,CBS-QB3}}$. The statistical errors are

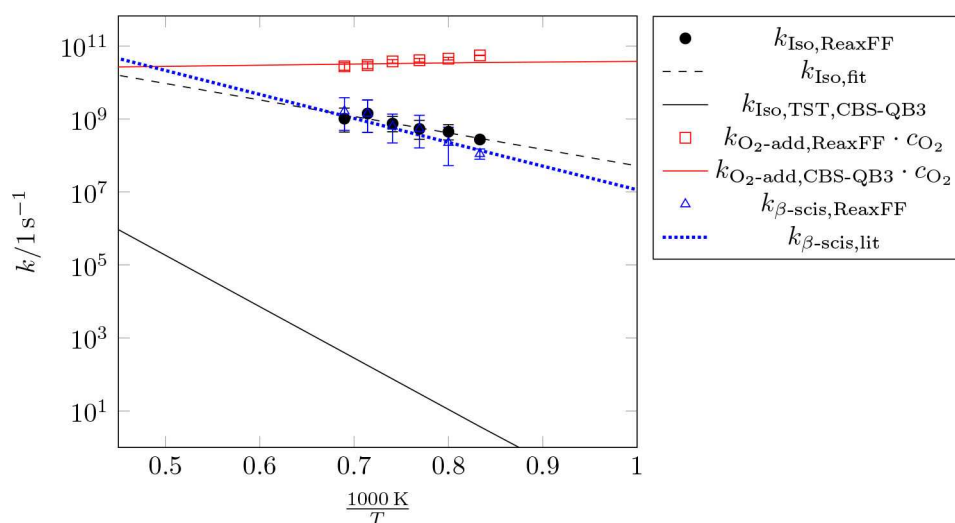


Figure 6. (Pseudo-) first-order reaction rate constants of the isomerization of the 2-pentyl radical to the iso-pentyl radical and the parallel reactions O₂-addition, and β -scission. k_{fit} is an Arrhenius fit to the data points from the trajectory. $k_{\text{O}_2\text{-add,CBS-QB3}}$ was obtained from Asatryan and Bozzelli,^[56] $k_{\beta\text{-scis,lit}}$ from Comandini et al..^[57]

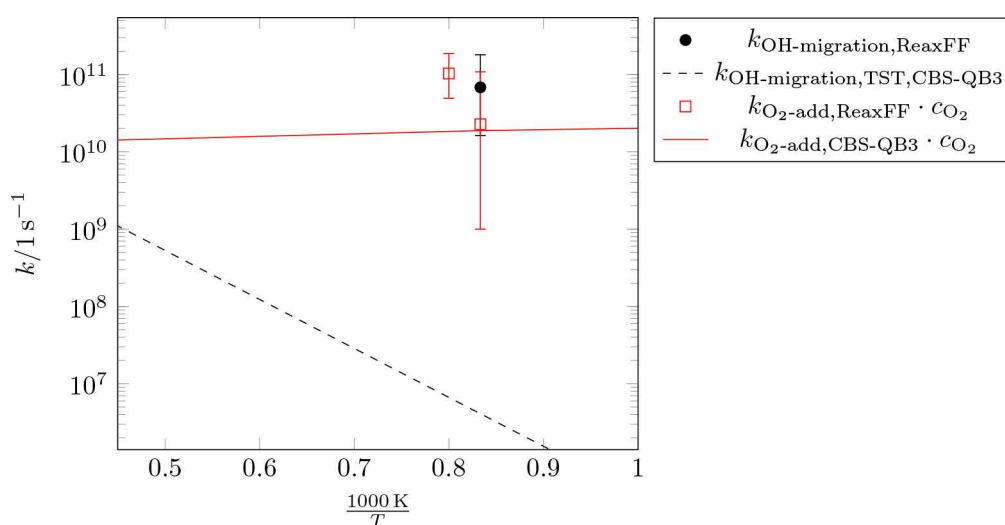


Figure 7. (Pseudo-) first-order reaction rate constants of the O₂-addition and the competing OH-migration of the 2-hydroperoxy-pent-4-yl radical. The CBS-QB3 O₂-addition high-pressure reaction rate constant is taken from Asatryan and Bozzelli.^[56]

too small to be the cause of the deviation. The lower slope of the Arrhenius fit to the data points from the trajectory $k_{\text{iso,fit}}$ compared to the CBS-QB3 TST reaction rate constant shows that the deviation is caused by a too low reaction barrier. The too low ReaxFF reaction barrier of approx. $15.3 \text{ kcal mol}^{-1}$ instead of $60.71 \text{ kcal mol}^{-1}$ on the CBS-QB3 level of theory makes the isomerization competing to the β -scission. The O_2 -addition is two orders of magnitude faster than both the isomerization and the β -scission at 1200 K. Both the O_2 -addition reaction rate constants $k_{\text{O}_2\text{-add,ReaxFF}}$ and the β -scission reaction rate constants $k_{\beta\text{-scis,ReaxFF}}$ have met the reaction rate constants from the literature ($k_{\text{O}_2\text{-add,CBS-QB3}}$, $k_{\beta\text{-scis,lit}}$) almost within statistical uncertainty (cf. Figure 6).

Further down the low-temperature reaction path, most $\text{ROO}\cdot$ species isomerize via internal H-atom abstractions. A minority reacts to alkenes and $\text{HO}_2\cdot$ radicals, decomposes into ketones and $\cdot\text{OH}$ radicals, or decomposes into radicals and diradicals ("bond dissociations" in Figure 5). The bond dissociations appear at multiple steps in the low-temperature path, e.g. reactions R54, R143, R157 in the Supporting Information. Neither the bond dissociations nor the formation of ketones or aldehydes and $\cdot\text{OH}$ radicals are included in the reference model (cf. "n/a" in Figure 5), but the latter have been described in the literature.^[84,85]

After the first internal H-atom abstraction, 18% of $\text{QOOH}\cdot$ species undergo the second O_2 -addition. In the reference model, though, this is the main reaction channel with a branching ratio of 78%. The main difference comes from the $\cdot\text{OH}$ -migration reaction $\text{QOOH}\cdot \rightarrow \cdot\text{QOOH}$. $\cdot\text{OH}$ -migration is not included in the reference model. Figure 7 illustrates that in our simulations, the $\cdot\text{OH}$ -migration and the O_2 -addition are competing. While the pseudo-first-order reaction rate constant of the O_2 -addition of the 2-hydroperoxide-pent-4-yl radical to 2-hydroperoxide-4-peroxide-pentane has been met almost within

statistical uncertainty (cf. $k_{\text{O}_2\text{-add,ReaxFF}} \cdot C_{\text{O}_2}$, $k_{\text{O}_2\text{-add,CBS-QB3}} \cdot C_{\text{O}_2}$ in Figure 7), the MD reaction rate constant of the $\cdot\text{OH}$ -migration $k_{\text{OH-migration,ReaxFF}}$ of the same molecule is too high by four orders of magnitude compared to the CBS-QB3 TST reaction rate constant $k_{\text{OH-migration,TST,CBS-QB3}}$. Again, the deviation can be explained by the too low ReaxFF energy barrier of approx. $5.33 \text{ kcal mol}^{-1}$ compared to approx. $28.44 \text{ kcal mol}^{-1}$ on the CBS-QB3 level of theory. Green et al.^[86] and Villano et al.^[87] discuss the $\cdot\text{OH}$ -migration reaction channel. Green et al.^[86] found that "this channel has a significant rate", but the competing cyclic-ether+ $\cdot\text{OH}$ formation is about an order of magnitude faster. The authors state that a final assessment of the importance of this $\cdot\text{OH}$ -migration channel is only possible by taking into account subsequent reactions of $\cdot\text{QOOH}$.^[86] Similar to the well-known $\text{RO}\cdot$ species,^[49] we have found that $\cdot\text{QOOH}$ decomposes into aldehydes and alkyl radicals via β -scission but also isomerizes into ethers (cf. Figure 8). Other $\cdot\text{QOOH}$ side reactions are the well-known cyclic ether formation, β -scissions, and formations of alkenes+ $\cdot\text{OH}$ (cf. Figure 5). Again, we observed bond dissociations, and formations of di-methyl-cyclopropane+ $\text{HO}_2\cdot$ (cyclic alkanes+ $\text{HO}_2\cdot$ in Figure 5). We found the latter reaction neither in the reference model nor in the literature. From the literature model, the products of the second O_2 -addition are expected to undergo a second internal H-atom abstraction in 79% of all cases (cf. Figure 5). Instead, we find a branching ratio of 27% in our simulations. Again, the main difference comes from a reaction that has not been included in the reference model. Asatryan and Bozzelli^[56] describe the barrierless carbonyl-peroxide+ $\cdot\text{OH}$ formation that can further decompose in a number of ways. They describe the decomposition of carbonyl-peroxides into oxygen, propene (we found a propyl radical, cf. Figure 9) and acetaldehyde, the elimination of $\text{CH}_3\cdot$, and the formation of oxetanes with the elimination of O_2 , a reaction that we did not observe. Instead, we found a ring

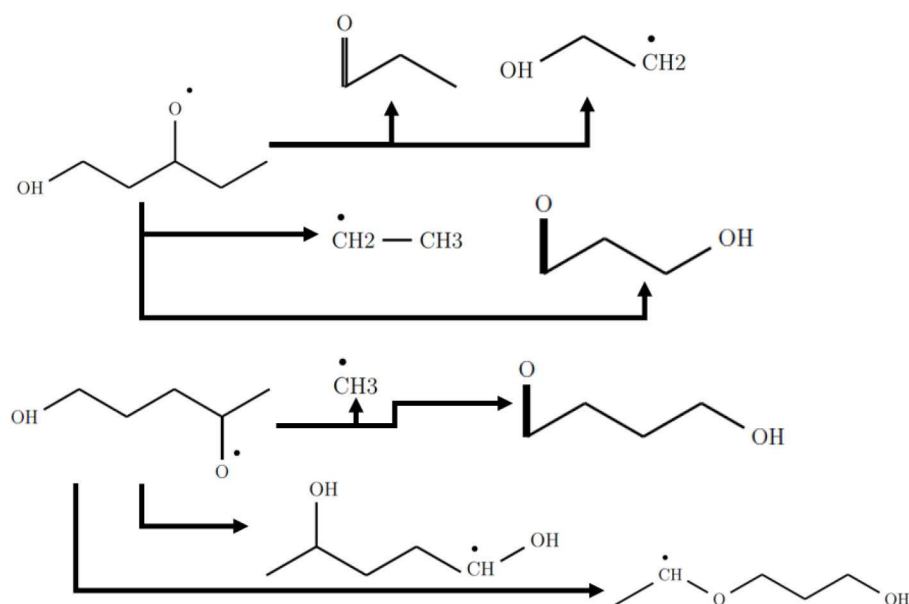


Figure 8. Examples of observed reactions of $\text{QOOH}\cdot$.

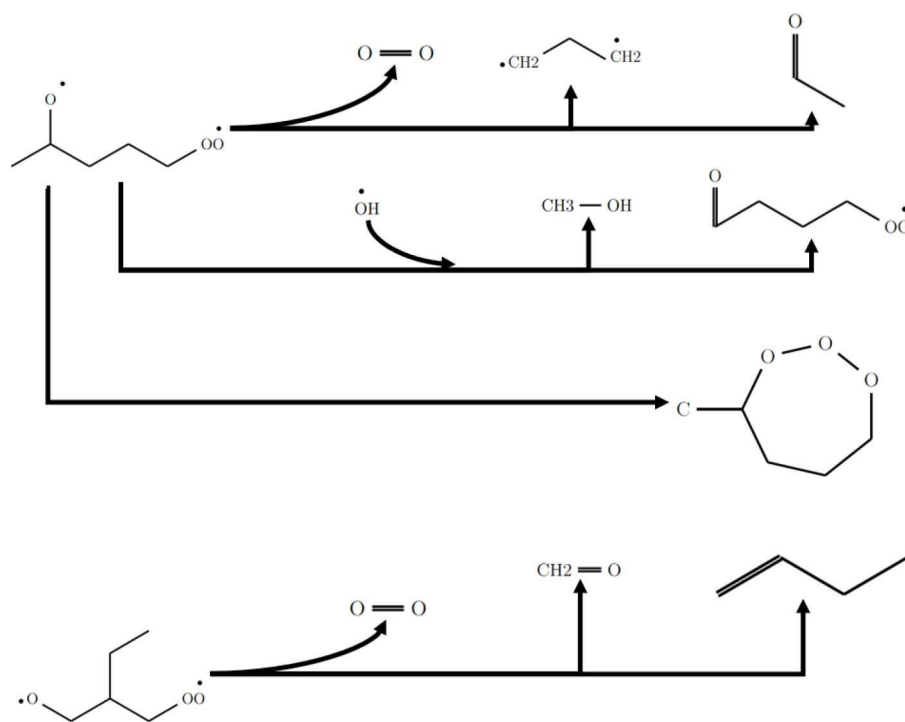


Figure 9. Examples of observed reactions of carbonyl-peroxides.

closure connecting the carbonyl radical site and the peroxy radical site (cf. Figure 9). A comparison of reaction rate constants of the carbonyl-peroxide + $\dot{\text{O}}\text{H}$ formation from our simulations and from the literature can be found in the Supporting Information.

After the second internal H-atom abstraction, 67% of HOOPOOH species in our simulations or 74% in the literature model, respectively, decompose into keto-hydroperoxides and $\dot{\text{O}}\text{H}$ radicals. Other side reactions than the formation of alkenes and HO_2 radicals side have not been observed.

We have shown that the major differences between our ReaxFF simulations and the reference model start with the $\dot{\text{Q}}\text{OOH}$ species in Figure 5 as the second O_2 -addition channel is less pronounced in our simulations than suggested by the reference model. The second O_2 -addition channel is diminished by the large number of $\dot{\text{Q}}\text{OOH}$ side reactions, which reduce the number of $\dot{\text{Q}}\text{OOH}$ species that can undergo the second O_2 -addition. Also, the computation of the reaction equilibria of the first and second O_2 -additions is computationally expensive, as the system spends much time hopping back and forth between the reactant and the product state. With high concentration, the representation of the reaction equilibria remains expensive, but, as the meta-stable O_2 -addition reaction equilibria are pushed to the product side, and subsequent reactions are accelerated by high temperature, the remaining simulation time is not only sufficient to observe the remaining key low-temperature reactions but also to observe a variety of verified side reactions.

3. Conclusions

With pAD, an acceleration method has been presented that allows for the simulation of low-temperature ignition processes, which are dominated by meta-stable O_2 -addition reaction equilibria, and internal H-atom abstractions. The method offers a physically substantiated way to increase the probability of escaping meta-stable reaction equilibria. While working without a bias, a suitable choice of parameters as ϕ , c_{O_2} , and temperature can optimize pAD performance. With only little information on 3 reactions, which are commonly known to be important in ignition processes, the three parameters could be tuned to increase visibility of the key low-temperature reactions in our pentane low-temperature ignition test case. The observed pathways were verified against an established pentane ignition reaction model from the literature.^[5–7] In addition to the key low-temperature reaction pathways, other reaction classes not included in that literature model,^[5–7] such as $\dot{\text{O}}\text{H}$ -migration or the formation of carbonyl-peroxides, showed up in the simulations. The applicability of pAD is not restricted to the low-temperature ignition process, but pAD can be employed more generally in cases in which association reactions in the gas phase play an important role.

Supporting Information

A list of all reactions including reaction rate constants derived from MD trajectories, as well as geometries of the 2-pentyl \rightarrow iso-pentyl radical isomerization and the 2-peroxide-pent-4-yl

$\dot{O}H$ -migration, a comparison of reaction rate constants of the carbonyl-peroxide + $\dot{O}H$ formation from our simulations and from the literature, and the employed schemes for the propagation of errors in energies to TST reaction rate constants, and to branching ratios are available in the Supporting Information. Also, a plot, in which experimental ignition delay times of different fuels are compared, is provided.

Acknowledgment

Financial support from the Deutsche Forschungsgemeinschaft (German Research Association) through Grant LE 2221/8 is gratefully acknowledged. Simulations were performed with computing resources granted by RWTH Aachen University under project rwth0281.

Conflict of Interest

The authors declare no conflict of interest.

Keywords: ChemTraYzer · ReaxFF · acceleration methods · low-temperature ignition · pentane

- [1] S. Vranckx, K. A. Heufer, C. Lee, H. Olivier, L. Schill, W. A. Kopp, K. Leonhard, C. A. Taatjes, R. X. Fernandes, *Combust. Flame* **2011**, *158*, 1444–1455.
- [2] J. Zador, C. A. Taatjes, R. X. Fernandes, *Prog. Energy Combust. Sci.* **2011**, *37*, 371–421.
- [3] G. Yang, E. A. Pidko, E. J. Hensen, *J. Catal.* **2012**, *295*, 122–132.
- [4] M. L. Coote, E. I. Izgorodina, G. E. Cavigliasso, M. Roth, M. Busch, C. Barner-Kowollik, *Macromolecules* **2006**, *39*, 4585–4591.
- [5] J. Bugler, K. P. Somers, E. J. Silke, H. J. Curran, *J. Phys. Chem. A* **2015**, *119*, 7510–7527.
- [6] J. Bugler, B. Marks, O. Mathieu, R. Archuleta, A. Camou, C. Grégoire, K. A. Heufer, E. L. Petersen, H. J. Curran, *Combust. Flame* **2016**, *163*, 138–156.
- [7] J. Bugler, A. Rodriguez, O. Herbinet, F. Battin-Leclerc, C. Togbé, G. Dayma, P. Dagaut, H. J. Curran, *Proc. Combust. Inst.* **2017**, *36*, 441–448.
- [8] E. Ranzi, A. Frassoldati, R. Grana, A. Cuoci, T. Faravelli, A. Kelley, C. Law, *Prog. Energy Combust. Sci.* **2012**, *38*, 468–501.
- [9] C. W. Gao, J. W. Allen, W. H. Green, R. H. West, *Comput. Phys. Commun.* **2016**, *203*, 212–225.
- [10] P. L. Bhoorasingh, B. L. Slakman, F. Seyedzadeh Khanshan, J. Y. Cain, R. H. West, *J. Phys. Chem. A* **2017**, *121*, 6896–6904.
- [11] V. Warth, F. Battin-Leclerc, R. Fournet, P. Glaude, G. Côme, G. Scacchi, *Comput. Chem.* **2000**, *24*, 541–560.
- [12] S. Rangarajan, A. Bhan, P. Daoutidis, *Ind. Eng. Chem. Res.* **2010**, *49*, 10459–10470.
- [13] R. V. de Vijver, K. M. V. Geem, G. B. Marin, J. Zádor, *Combust. Flame* **2018**, *196*, 500–514.
- [14] M. Bergeler, G. N. Simm, J. Proppe, M. Reiher, *J. Chem. Theory Comput.* **2015**, *11*, 5712–5722.
- [15] Y. Kim, J. W. Kim, Z. Kim, W. Y. Kim, *Chem. Sci.* **2018**.
- [16] P. M. Zimmerman, *J. Comput. Chem.* **2013**, *34*, 1385–1392.
- [17] P. M. Zimmerman, *Mol. Simul.* **2015**, *41*, 43–54.
- [18] A. L. Dewyer, P. M. Zimmerman, *Org. Biomol. Chem.* **2017**, *15*, 501–504.
- [19] Y. V. Suleimanov, W. H. Green, *J. Chem. Theory Comput.* **2015**, *11*, 4248–4259.
- [20] S. Habershon, *J. Chem. Phys.* **2015**, *143*, 094106.
- [21] A. L. Dewyer, A. J. Argüelles, P. M. Zimmerman, *WIREs Comput. Mol. Sci.* **2018**, *8*, e1354.
- [22] M. Döntgen, F. Schmalz, W. A. Kopp, L. C. Kröger, K. Leonhard, *J. Chem. Inf. Model.* **2018**, *58*, 1343–1355.
- [23] S. Maeda, K. Ohno, *J. Phys. Chem. A* **2005**, *109*, 5742–5753.
- [24] S. Maeda, K. Ohno, *J. Phys. Chem. A* **2005**, *109*, 5742–5753.
- [25] S. Maeda, K. Ohno, K. Morokuma, *Phys. Chem. Chem. Phys.* **2013**, *15*, 3683–3701.
- [26] A. F. Voter, *Phys. Rev. Lett.* **1997**, *78*, 3908–3911.
- [27] A. Laio, F. L. Gervasio, *Rep. Prog. Phys.* **2008**, *71*, 126601.
- [28] R. A. Miron, K. A. Fichthorn, *J. Chem. Phys.* **2003**, *119*, 6210–6216.
- [29] K. M. Bal, E. C. Neyts, *J. Chem. Theory Comput.* **2015**, *11*, 4545–4554.
- [30] M. R. Sørensen, A. F. Voter, *J. Chem. Phys.* **2000**, *112*, 9599–9606.
- [31] R. J. Allen, P. B. Warren, P. R. ten Wolde, *Phys. Rev. Lett.* **2005**, *94*, 018104.
- [32] R. J. Allen, D. Frenkel, P. R. ten Wolde, *J. Chem. Phys.* **2006**, *124*, 024102.
- [33] R. J. Allen, P. Valeriani, C. Rein ten Wolde, *J. Phys. Condens. Matter* **2009**, *21*, 463102.
- [34] K. Kratzer, J. T. Berryman, A. Taudt, J. Zeman, A. Arnold, *Comput. Phys. Commun.* **2014**, *185*, 1875–1885.
- [35] A. F. Voter, *Phys. Rev. B* **1998**, *57*, R13985–R13988.
- [36] K. L. Joshi, S. Raman, A. C. T. van Duin, *J. Phys. Chem. Lett.* **2013**, *4*, 3792–3797.
- [37] S. Ghosh, K. Jana, B. Ganguly, *Phys. Chem. Chem. Phys.* **2019**, *21*, 13578–13589.
- [38] V. M. Miriyala, R. Lo, S. Haldar, A. Sarmah, P. Hobza, *J. Phys. Chem. C* **2019**, *123*, 14712–14724.
- [39] V. Rizzi, D. Polino, E. Sicilia, N. Russo, M. Parrinello, *Angew. Chem. Int. Ed.* **2019**, *58*, 3976–3980.
- [40] S. Chakraborty, S. Ghosh, *Comp. Mater. Sci.* **2018**, *154*, 212–224.
- [41] B. P. Uberuaga, R. Perriot, G. Pilania, *Phys. Chem. Chem. Phys.* **2019**, *21*, 5956–5965.
- [42] L. Luo, W. Ma, Y. Zhuang, Y. Zhang, S. Yi, J. Xu, Y. Long, D. Ma, Z. Zhang, *Ecol. Indic.* **2018**, *93*, 24–35.
- [43] E. Martínez, R. Perriot, E. M. Kober, P. Bown, M. Powell, S. McGrane, M. J. Cawkwell, *J. Chem. Phys.* **2019**, *150*, 244108.
- [44] F. Hédin, T. Lelièvre, *Comput. Phys. Commun.* **2019**, *239*, 311–324.
- [45] A. Vashisth, C. Ashraf, W. Zhang, C. E. Bakis, A. C. T. van Duin, *J. Phys. Chem. A* **2018**, *122*, 6633–6642.
- [46] B. M. Dickson, *J. Chem. Theory Comput.* **2019**, *15*, 78–83.
- [47] C. Wehmeyer, F. Noé, *J. Chem. Phys.* **2018**, *148*, 241703.
- [48] V. P. Zhukov, *Combust. Theory Modell.* **2009**, *13*, 427–442.
- [49] H. Curran, P. Gaffuri, W. Pitz, C. Westbrook, *Combust. Flame* **1998**, *114*, 149–177.
- [50] D. G. Goodwin, H. K. Moffat, R. L. Speth, “Cantera: An Object-oriented Software Toolkit for Chemical Kinetics, Thermodynamics, and Transport Processes”, <http://www.cantera.org>, **2017**, Version 2.3.0.
- [51] L.-P. Wang, A. Titov, R. McGibbon, F. Liu, V. S. Pande, T. J. Martínez, *Nat. Chem.* **2014**, *6*, 1044–1048.
- [52] C. Ashraf, A. C. T. van Duin, *J. Phys. Chem. A* **2017**, *121*, 1051–1068.
- [53] S. Grimme, *J. Chem. Theory Comput.* **2019**, *15*, 2847–2862.
- [54] K. M. Bal, E. C. Neyts, *Chem. Sci.* **2016**, *7*, 5280–5286.
- [55] K. Chenoweth, A. C. T. van Duin, W. A. Goddard III, *J. Phys. Chem. A* **2008**, *112*, 1040–1053.
- [56] R. Asatryan, J. W. Bozzelli, *J. Phys. Chem. A* **2010**, *114*, 7693–7708.
- [57] A. Comandini, I. A. Awan, J. A. Manion, *Chem. Phys. Lett.* **2012**, *552*, 20–26.
- [58] L. C. Kröger, W. A. Kopp, M. Döntgen, K. Leonhard, *J. Chem. Theory Comput.* **2017**, *13*, 3955–3960.
- [59] A. Sudholt, C. Lee, J. Klankermayer, R. X. Fernandes, H. Pitsch, *Combust. Flame* **2016**, *171*, 133–136.
- [60] U. Burke, K. P. Somers, P. O’Toole, C. M. Zinner, N. Marquet, G. Bourque, E. L. Petersen, W. K. Metcalfe, Z. Serinyel, H. J. Curran, *Combust. Flame* **2015**, *162*, 315–330.
- [61] D. Healy, N. Donato, C. Aul, E. Petersen, C. Zinner, G. Bourque, H. Curran, *Combust. Flame* **2010**, *157*, 1526–1539.
- [62] L. Martínez, R. Andrade, E. G. Birgin, J. M. Martínez, *J. Comput. Chem.* **2009**, *30*, 2157–2164.
- [63] H. Aktulga, J. Fogarty, S. Pandit, A. Grama, *Parallel Comput.* **2012**, *38*, 245–259.
- [64] S. Plimpton, *J. Comput. Phys.* **1995**, *117*, 1–19.
- [65] M. Döntgen, M.-D. Przybylski-Freund, L. C. Kröger, W. A. Kopp, A. E. Ismail, K. Leonhard, *J. Chem. Theory Comput.* **2015**, *11*, 2517–2524.
- [66] J. Ding, L. Zhang, Y. Zhang, K.-L. Han, *J. Phys. Chem. A* **2013**, *117*, 3266–3278.
- [67] F. Castro-Marciano, A. C. van Duin, *Combust. Flame* **2013**, *160*, 766–775.
- [68] A. Bharti, T. Banerjee, *Fuel Process. Technol.* **2016**, *152*, 132–139.
- [69] X.-M. Cheng, Q.-D. Wang, J.-Q. Li, J.-B. Wang, X.-Y. Li, *J. Phys. Chem. A* **2012**, *116*, 9811–9818.

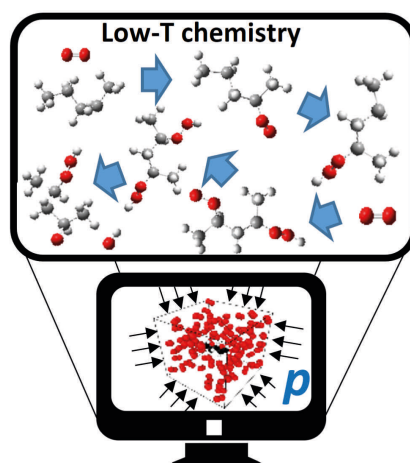
- [70] F. Castro-Marciano, A. M. Kamat, M. F. Russo, A. C. van Duin, J. P. Mathews, *Combust. Flame* **2012**, *159*, 1272–1285.
- [71] M. Zheng, X. Li, J. Liu, Z. Wang, X. Gong, L. Guo, W. Song, *Energ. Fuel* **2014**, *28*, 522–534.
- [72] T. Zhang, X. Li, X. Qiao, M. Zheng, L. Guo, W. Song, W. Lin, *Energ. Fuel* **2016**, *30*, 3140–3150.
- [73] S. G. Srinivasan, A. C. T. van Duin, *J. Phys. Chem. A* **2011**, *115*, 13269–13280.
- [74] P. Ganesh, P. R. C. Kent, V. Mochalin, *J. Appl. Phys.* **2011**, *110*, 073506.
- [75] L. Goerigk, A. Hansen, C. Bauer, S. Ehrlich, A. Najibi, S. Grimme, *Phys. Chem. Chem. Phys.* **2017**, *19*, 32184–32215.
- [76] A. Ghysels, T. Verstraelen, K. Hemelsoet, M. Waroquier, V. Van Speybroeck, *J. Chem. Inf. Model.* **2010**, *50*, 1736–1750.
- [77] X. Li, M. J. Frisch, *J. Chem. Theory Comput.* **2006**, *2*, 835–839.
- [78] J. A. Montgomery, M. J. Frisch, J. W. Ochterski, G. A. Petersson, *J. Chem. Phys.* **1999**, *110*, 2822–2827.
- [79] J. A. Montgomery, M. J. Frisch, J. W. Ochterski, G. A. Petersson, *J. Chem. Phys.* **2000**, *112*, 6532–6542.
- [80] J. Zheng, Y. Zhao, D. G. Truhlar, *J. Chem. Theory Comput.* **2009**, *5*, 808–821.
- [81] W. A. Kopp, R. T. Langer, M. Döntgen, K. Leonhard, *J. Phys. Chem. A* **2013**, *117*, 6757–6770.
- [82] J. Pieper, C. Hemken, R. Büttgen, I. Graf, N. Hansen, K. A. Heufer, K. Kohse-Höinghaus, *P. Combust. Inst.* **2019**, *37*, 1683–1690.
- [83] J. Proppe, T. Husch, G. N. Simm, M. Reiher, *Faraday Discuss.* **2016**, *195*, 497–520.
- [84] C. F. Goldsmith, W. H. Green, S. J. Klippenstein, *J. Phys. Chem. A* **2012**, *116*, 3325–3346.
- [85] H. Jin, J. Pieper, C. Hemken, E. Bräuer, L. Ruwe, K. Kohse-Höinghaus, *Combust. Flame* **2018**, *193*, 36–53.
- [86] W. H. Green, C. D. Wijaya, P. E. Yelvington, R. Sumathi, *Mol. Phys.* **2004**, *102*, 371–380.
- [87] S. M. Villano, L. K. Huynh, H.-H. Carstensen, A. M. Dean, *J. Phys. Chem. A* **2012**, *116*, 5068–5089.

Manuscript received: September 9, 2019

Version of record online: ■■■, ■■■■

ARTICLES

Time to ignite: The low-temperature ignition reaction process exceeds the time scales accessible to reactive Molecular Dynamics simulations. Through a drastic increase of pressure, the important reactions can be made visible within the accessible time scales. Compared to many other existing acceleration methods, only a minimum of *a-priori* knowledge is necessary for the successful application of the „pressure-accelerated dynamics“ method.



*L. Krep, Dr. W. A. Kopp, L. C. Kröger,
Dr. M. Döntgen, Prof. Dr. K. Leonhard**

1 – 11

**Exploring the Chemistry of Low-
Temperature Ignition by Pressure-
Accelerated Dynamics**

Special
Collection